J Appl Electrochem (2011) 41:39–49
DOI 10.1007/s10800-010-0205-8

ORIGINAL PAPER

Synergistic effect of additives on bright nanocrystalline zinc electrodeposition

K. O. Nayana · T. V. Venkatesha · B. M. Praveen · K. Vathsala

Received: 9 December 2009 / Accepted: 5 September 2010 / Published online: 19 September 2010

Abstract The influence of additives like cetyltrimethylammonium bromide (CTAB) and Ethyl vanillin (EV) on zinc electrodeposition from acid sulfate bath was systematically investigated by scanning electron microscopy, X-ray diffraction, and voltammetric techniques. The result shows the existence of interaction between CTAB and EV. They exhibited synergistic effect to produce bright nanocrystalline zinc coating on steel surface. The combined effects of these two compounds on deposition overpotential, hydrogen evolution, zinc ion diffusion, and surface coverage were discussed. The morphological and orientational changes occurred in electrodeposit were presented. Also the nucleation mechanism exhibited by zinc during electrodeposition in the presence of additive was examined.

Keywords Electrodeposition · Ethyl vanillin · Nanocrystalline · Nucleation mechanism · Synergistic effect

1 Introduction

Bright zinc coating on steel provides a sacrificial protection against corrosion and is one of the major methods for protecting steel in industries. On an industrial scale the zinc electrodeposition is obtained from alkaline cyanide baths. But due to high toxic nature of cyanide baths, other baths like sulfate, chloride and sulphamate are gaining importance even though they have poor throwing power [1–6]. The primary goal of all these baths is to generate quality zinc deposit with good corrosion protection ability to steel. The corrosion resistant property of zinc deposit depends mainly on its fine grained nature, smoothness, levelling and degree of brightness. All these potential properties of zinc deposit are achieved through the use of optimized and balanced amount of bath constituents. The important constituents of plating baths are metal ions, conducting salts, buffering agents and organic additives. Among these only the additives play a prominent role in producing bright deposit with improved quality. Examining the earlier work on this subject revealed that all zinc plating baths are associated with two or more additives and their effect on bright deposition is more pronounced when used in combination [7–13]. The primary role of these additives is to influence the factors affecting deposition process so as to get a bright coating on the substrate. Numerous literatures are available on electroplating of pure zinc. In most of the study, considerable attention has been directed toward the development of effective additives/brighteners to generate smooth and leveled bright deposit capable of providing higher corrosion resistance. A few researchers have attempted to explain the role, mechanism, and functions of additives on parameters affecting electrodeposition process of bright coating [14].

These additives are classified as primary and secondary, which always in combination produce bright deposit on an initially dull substrate or which maintains brightness on an initially bright substrate [15]. Most of the primary additives are surfactants (wetting agents, levellers, and grain refiners) whereas secondary additives [brighteners] are organic compounds like aromatic and aliphatic aldehydes, ketones, sulfur containing compounds, and alkyl and aryl ammonium salts [14–18].

K. O. Nayana · T. V. Venkatesha (✉) · B. M. Praveen · K. Vathsala
Department of PG Studies and Research in Chemistry, Kuvempu University, Shankaraghatta 577 451, India
e-mail: drtvvenkatesha@yahoo.co.uk

The primary additive imparts leveling and smoothness to deposit. The typical examples are cationic (CTAB—cetyltrimethylammonium bromide), anionic (SDS—sodium dodecylsulfate), and nonionic (Triton X-100, poly ethylene glycols PEG) surfactants [12–21]. Cationic surfactant-like CTAB with positively charged head group interacts electrostatically with the electrode surface and thus get adsorbed on the active sites, modifying the crystal growth mode, tailors the morphology and refining grain size of the deposit [18].

The secondary additives such as benzylideneacetone [17], vanillin [14], furfuraldehyde [22], polyacrylamine [23], etc. are reported as brighteners for zinc deposition. These secondary additives interact synergistically with primary additive giving mirror bright finishing. Synergistic action exerted by mixture of additives enhances interaction between them and their adsorption (or incorporation) in the deposit [24].

Loshkare and co-workers investigated the combined effect of thiourea and OP-10 (a polymeric species) and showed that the combined effect is much higher than their individual effect [7, 8]. Moucheng Li et al. in their study concluded that a bright and compact zinc coating with a grain size of 43 nm and (110)(100)(201) preferred orientation are produced due to the co-existence of all four compounds CTAB, PEG, benzalacetone, and thiourea [9].

The effect of benzoic acid (BA) and PEG on initial stages of zinc electrodeposition on iron electrode was investigated by cyclic voltammetric studies and concluded that when both BA and PEGs are present, they interact closely with each other and show an intermediate behavior [10, 11]. The influence of nonionic surfactant and benzylideneacetone (BDA) on zinc electrodeposition is studied and established that the BDA transformed into different compounds at the cathode. These products associate and occupy a larger area at the cathode surface than any of the additives used alone and thus produce synergistic effect [12]. Li et al. reported the synergistic effect of thiourea and benzalacetone in reducing the grain size of zinc coating. This is due to the combined effect which increased the overpotential, retarded the continuous grain growth, and increased nucleation rate [13, 25, 26]. All these earlier studies revealed that the generation of a bright, compact zinc deposition is possible only from electrolytes containing two or more specific additives. Reviewing these results it is inferred that the additives are able to produce a bright deposit only when (a) they are adsorbed on cathode surface, (b) they block the active sites, (c) affect the preferred orientation, (d) undergo electrochemical changes at the cathode surface, (e) increase deposition overpotential, (f) retard the grain growth, and (g) increase the nucleation density. All these factors are fulfilled through the combined application of two or more additives.

Further, the detailed literature search indicated not much work on explaining the synergistic effect of additives on bright zinc deposition. This study is focused on the study of synergistic effect of CTAB and ethyl vanillin (EV) mixture on bright zinc deposition. Their influence on nucleation mode, morphology, and texture of the deposit were investigated by cyclic voltammetry, XRD, and SEM analysis.

2 Experimental

The analytical grade chemicals (s d-fine, Mumbai, India) and Millipore water (US) were used to prepare bath solutions. The mild steel panel of 4 × 4 cm^2 area was used as cathode. The surface of mild steel panel was mechanically polished, degreased by vapors of trichloroethylene in degreaser plant, and immersed for 5 min in 10% HCl to remove dust and rust. The panel was then washed in running water and transferred to plating bath solution. The anode was zinc (99.9%) metal plate, and its surface was activated each time by dipping in 10% HCl for few seconds followed by water wash.

The composition of the bath solutions used for zinc electrodeposition was given in Table 1. The deposit on steel was obtained at 25 mA cm^{-2} current density using DC power supply (PS-618 potentiostat/galvanostat), and the deposition time was 20 min (thickness 14 μm).

Morphology of the deposit in the presence and absence of additives was analyzed by scanning electron microscope (FESEM, LE01530-VP) images. Also grain size and crystal orientations were examined by X-ray diffraction (XRD) studies. The average grain size was evaluated by Debye Scherer's equation $D = k\lambda/\beta\cos\theta$. Where, $k = 0.9$, β is the full width at half maximum, θ is the reflectance angle, and $\lambda = 1.546$ Å is the wavelength of radiations used [27].

The preferred orientations of the deposits were determined by using Muresan's method by calculating the texture coefficient (T_C) with the equation:

$$T_C(hkl) = \frac{I(hkl)}{\sum I(hkl)} \times \frac{\sum I_0(hkl)}{I_0(hkl)} \times 100 \quad (1)$$

where I (hkl) is the peak intensity of zinc electrodeposits and ΣI is the sum of the intensities of independent peaks.

Table 1 Zinc plating bath

Components	Bath (M)			
	I	II	III	IV
$ZnSO_4{\cdot}7H_2O$	0.68	0.68	0.68	0.68
Na_2SO_4	0.28	0.28	0.28	0.28
H_3BO_3	0.19	0.19	0.19	0.19
CTAB	–	0.005	–	0.005
EV	–	–	0.004	0.004

The index 0 refers to the intensities for the standard zinc sample (JCPDS card number: 00-004-0831) [28].

Electrochemical studies were carried out in a conventional three-electrode cell. The working electrode was stainless steel (SS101) disk of surface area 0.0774 cm^2 enclosed in a Teflon tube. The surface was polished to mirror finish using emery paper (1200 grit) with 0.05 μm alumina and activated in a solution of 30% hydrochloric acid solution followed by water wash. The saturated calomel electrode (SCE) and a Pt wire were employed as reference and counter electrode, respectively. For all electrochemical measurements CHI660C electrochemical analyzer (USA) was used. Each curve in the cyclic voltammogram was corrected for ohmic potential drop obtained from the high-frequency electrode impedance.

Electro-active surface area of the SS101 stainless steel electrode was determined to be 0.0719 cm^2 by using an aqueous solution of 10 mM $ZnSO_4{\cdot}7H_2O$ in 1M KCl and diffusion coefficient, $D_{(1/2Zn^{+2})} = 7.03 \times 10^{-6}\ cm^2\ s^{-1}$ [29]. The roughness factor (RF) of the electrode was calculated by using relation $RF =$ electro-active surface area/geometric surface area. Here the geometric area of electrode was 0.0774 cm^2 and RF value was 0.928. The measured electro-active surface area was in good agreement with the geometrical area.

For deposition and morphological studies, the plating bath solutions given in Table 1 were used. The plating conditions and bath constituents are optimized by Hull cell studies.

For voltammetric analysis the electrolytes used were $S_O = 0.34M\ ZnSO_4{\cdot}7H_2O$, 1M Na_2SO_4, 0.08M H_3BO_3, $S_C = S_O + 0.0025$ M CTAB, $S_E = S_O + 2$ mM EV, $S_{CE} = S_O + 0.0025$ M CTAB + 2 mM EV at temperature 300 K pH 2.8 adjusted with 1M H_2SO_4 and $NaHCO_3$.

3 Results and discussion

3.1 Morphology and crystal orientation

The SEM images recorded for zinc deposit, obtained from baths I to IV, given in Table 1. For the bath-I, the SEM image of the deposit in the form of stacks of hexagonal platelets is distributed randomly as shown in Fig. 1a. The Fig. 1b and c shows the SEM images for the deposit generated from the bath-II and III, respectively. There is a greater refinement in grain size producing granules of uniform size and shape. These SEM images recorded for the deposit obtained in the presence of individual additives showed greater reduction in zinc deposit crystallites. Here the grains were distributed with higher degree of size uniformity. In the presence of both CTAB and EV, the deposit exhibits additional refinement in grain size with increased brightness as shown in Fig. 1d. The analysis of SEM images revealed that polycrystalline dull deposit converted into fine-grained nanocrystalline bright deposit.

The zinc deposit obtained from the bath-I shows grain size of 155.8 nm with 5% reflectance (dull deposit—Table 2). The XRD pattern for the deposit is presented in Fig. 2a and indicated (002) preferred orientation without line broadening. The texture coefficient (T_C) for the deposit is given in Table 3. The maximum T_C 43.1% for (002) orientation inferred that in the absence of additive, the zinc deposit crystallizes into (002) orientation [30]. These observations are in accordance with the similar peak intensities recorded by Gomes et al. [18] and Hsieh et al. [30] for zinc deposition on steel surface.

The bath-II gave a semibright nano-sized crystalline zinc coating with grain size of 72.9 nm and 22% reflectance. The Fig. 2b represents the XRD pattern of zinc deposit. The maximum T_C value of 55.5% obtained for (110) orientation indicated that (110) is the preferred orientation of the deposit. Hence zinc deposit in the presence of CTAB crystallizes into (110) preferred orientation [11, 19].

Almost similar type of deposit was noticed from bath-III with grain size of 70.07 nm and 68% reflectance. The XRD pattern in Fig. 2c corresponds to zinc deposit obtained from bath-III containing EV alone. The deposit is without significant preferred orientation. T_C values are comparatively not higher for any of the orientations. In the presence of EV, the deposit is semibright and nonuniform, which shows an average reflectance of 68% and smaller grain size (70.07 nm). The mixture of CTAB and EV in bath-IV produced bright, smooth zinc deposit on steel with grain size of 49.26 nm and 85% surface reflectance. The XRD pattern for this deposit is presented in Fig. 2d, and the peaks show line broadening. The Tc values which are maximum for (100) and (110) orientation and about 39.23 and 29.89%, respectively, inferred that (100) (110) are the preferred orientations of the deposit in the presence of both the additives as shown in Table 3. These observed results are in good agreement with the referred data in the literature [30]. The observed preferred orientation in deposit is likely to be resulted from the influence of additives. The crystals in the presence of additives adopt a preferred orientation as indicated by X-ray diffraction analysis. This preferred orientation arises due to different rates of growth of different faces of the crystal because of additive adsorption on cathode surface [31].

The observed crystal size of the deposit reduced from 155.8 nm (dull) to 49.26 nm (bright). Further the additives CTAB and EV when present individually in the bath give semi-bright deposit with grain size of 72.9 and 70.07 nm, respectively. Further, reduction in grain size to 49.26 nm (mirror bright) was noticed in the presence of both the

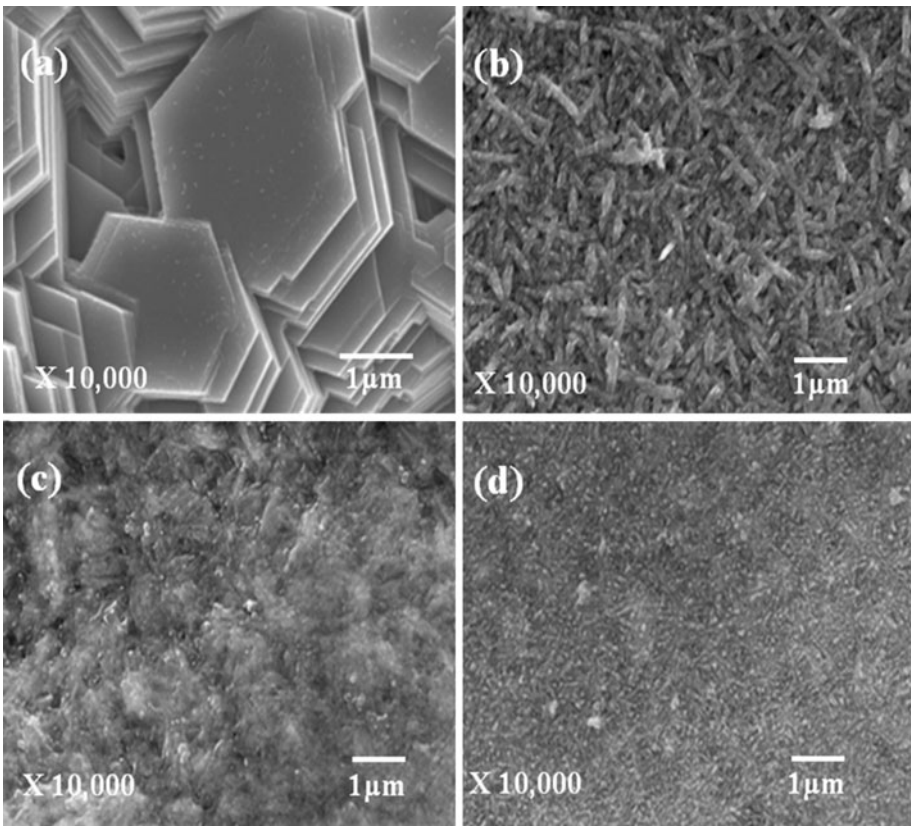

Fig. 1 SEM images of deposit obtained from bath **a** I, **b** II, **c** III, and **d** IV

Table 2 Grain size, reflectance, and appearance of deposit

Solution	I	II	III	IV
Average grain size (nm)	155.8	72.9	70.07	49.26
Reflectance (%)	05	22	68	85
Appearance	Dull	Semibright	Semibright	Bright

additives. The deposit that is smooth and defect-free implies the combined effect of addition agents.

The XRD and SEM studies of the zinc deposit revealed that the additives influence the parameters of deposition process thereby affecting the nature of the deposit. The above morphological and orientation change arises due to the presence of both additives, and hence, there exists some interaction between CTAB and EV by which they influence the electrodeposition process. In order to examine the influence of additives on zinc deposition process, voltammetric studies were under taken.

3.2 Voltammetric studies

3.2.1 Voltammetric studies in the absence of additives

Voltammogram recorded for solution S_O in the potential range from −0.5 to −1.4 V at scan rate of 50 mVs^{-1}, mainly consisting of peaks I_c, I'_c, and I_a as shown in Fig. 3.

Initial peak I_c of very small magnitude is observed between −0.5 and −1.0 V and is shown in Fig. 3b. The similar peak is also observed in the voltammograms recorded in the absence of Zn^{+2}. The peak current increased with fall in pH of S_O (voltammograms not shown) indicated hydrogen evolution ($2H_2O + 2e^- = H_2 + 2OH^-$), and the H_2 gas bubbles are observed visually at the cathode surface [32–34]. In this peak region, the formation of ZnH, ZnO, and ZnOH layers, which occurs during zinc deposition from acid sulfate bath, was reported in the literature [19]. Further, it reported that zinc deposit occurs at more negative potential than calculated equilibrium potential due to zinc hydroxide layer formation. In the present case also peak I'_c corresponds to bulk zinc reduction at higher negative potential, i.e., −1.315 V.

On reversing the sweep direction, two current crossovers appear in the cathodic region of voltammogram, which indicated three-dimensional (3D) nucleation and subsequent crystal growth [35]. The anodic peak (I_a) centered at −0.844 V is attributed to the oxidation of metallic Zn to Zn^{2+}.

The relation between cathodic peak current Ip (I'_c) and square root of scan rate ($v^{1/2}$) is shown in Fig. 3c. The linearity is noticed, and it inferred that the reduction processes are under diffusion control. However, the intercept higher than zero indicated an additional process other than diffusion [36].

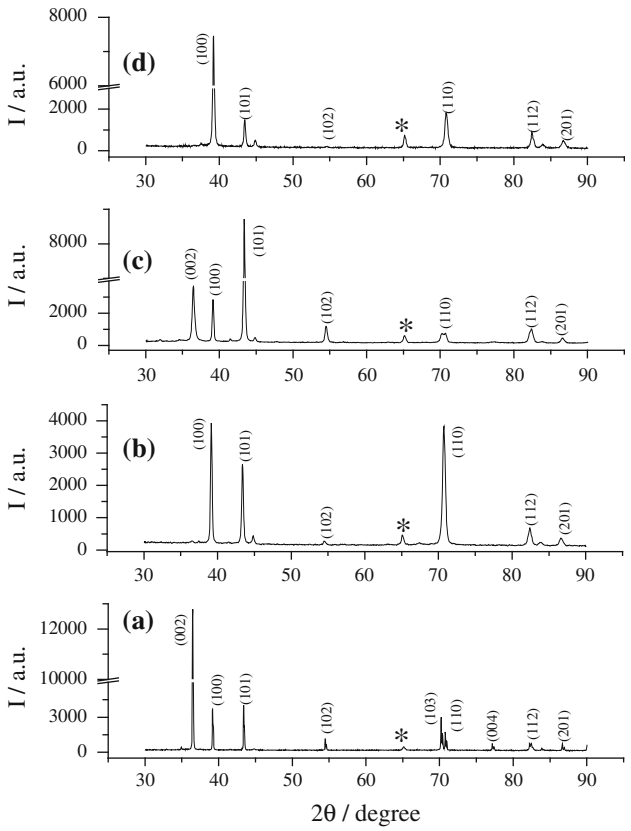

Fig. 2 XRD pattern of zinc deposit at 25 mA cm^{-2} obtained from bath **a** I, **b** II, **c** III, and **d** IV (*steel)

Table 3 Texture coefficient (T_c) of Zn deposits

Plane (*hkl*)	T_c (*hkl*)%			
	I	II	III	IV
(002)	43.1	0	17.5	0
(100)	0.6	18.4	12.91	39.23
(101)	0.3	5.5	17.97	2.99
(102)	0.6	1.2	10.0	0.54
(103)	0.7	0	0	0
(110)	12.2	55.5	9.5	29.89
(004)	25.5	0	0	0
(112)	9.2	7.4	13.7	9.0
(200)	0	7.3	18.3	10.89
(201)	7.8	4.9	0	7.46

To examine the type of kinetics control involved in deposition of zinc, voltammetric studies were carried out at different negative switching potential E_λ ($>E_{CO}$), wherein deposition process is not diffusion-controlled. Figure 4 shows that the crossover potential (E_{CO}) remains constant for different E_λ indicating that, in this condition, the electrodeposition process is controlled by charge transfer and follows Fletcher's theory [37]. The E_{CO} corresponding to equilibrium potential of metal/metal ion system ($E_{CO} = E^{o}_{M^{n+}/M}$) was found to be −1.095 V vs. S_{CE} (Fig. 4). This value is more negative than −1.024 V vs. S_{CE} which was calculated from Nernst equation for the system Zn^{2+}/Zn ($E_{Zn^{2+}/Zn} = -1.01–0.03\ pZn^{2+}$, zinc reduction reaction is $Zn^{2+} + 2e^- = Zn$). The slight difference of potential arises due to crystallization overpotential related to stainless steel substrate.

The examination of the anodic part of Fig. 4 revealed gradual reduction of anodic peak size when E_λ changes to less negative and also associated with negative shift of the peak potential indicating an easier dissolution of zinc deposit. The negative shift of anodic potential may also be due to smaller polarization of the electrode at less negative potential [38].

3.2.2 *Voltammetric studies in the presence of additives*

To study the effect of interaction of additives CTAB and EV on producing bright deposit the voltammetric studies were carried out in potential range from −0.5 to −1.7 V using electrolyte solutions S_C, S_E, and S_{CE}. The voltammograms were analyzed with reference to that of pure zinc solution S_O.

Figure 5a represents the cyclic voltammograms for zinc deposition from electrolyte in the presence and absence of additives. The peak potential is always more negative in the presence of additives for zinc deposition than their absence. This negative shift in peak potential in the presence of additive is due to the adsorption of additive on active sites. The shift in peak potentials toward cathodic direction is more pronounced for CTAB + EV mixture than they are present alone. The peak potentials are given in Table 4.

Figure 5b represents the enlarged potential region from −0.8 to −1.0 V. The CTAB and EV, individually and in combination, showed higher peak current (Fig. 5b) in comparison with S_O, i.e., without additives. This increase in the current density is due to higher rate of reduction of zinc ions in comparison with the hydrogen evolution, which is in accordance with the study reported by Gomes et al. [19]. Further in the presence of EV and EV + CTAB, the peak potential shifted to negative direction with simultaneous decrease in peak current when compared to CTAB alone. The zinc reduction in the presence of mixture is relatively less in the potential region from −0.8 to −1.0 V indicated their combined effect on reduction reaction. The same trend is noticed in peak current, for each additive, in the absence of Zn^{2+} in the same potential region, but the current is lower and is arising out of hydrogen evolution.

The blockage of electrode surface by the additives inhibits the zinc deposition process, which causes the decrease of voltammetric current in their presence. The

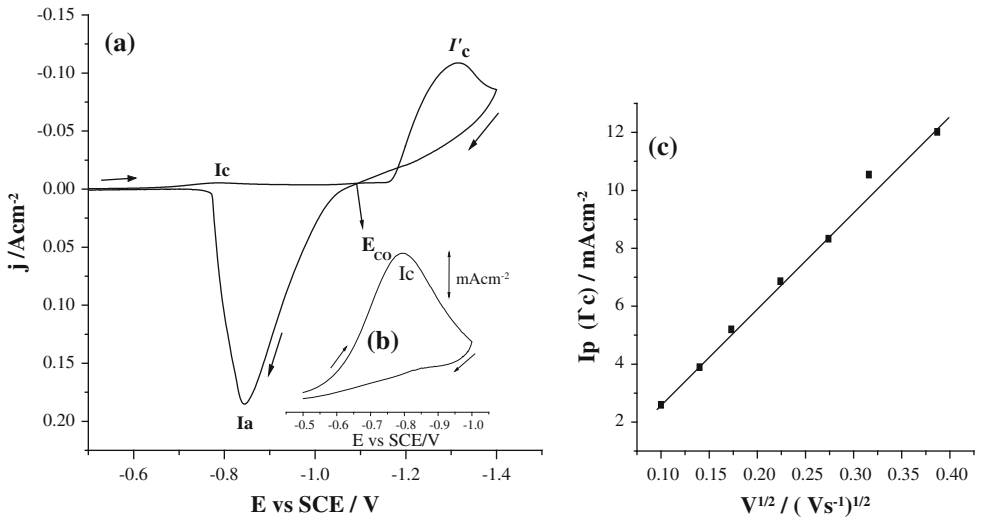

Fig. 3 Cyclic voltammograms for solution S_O on stainless steel electrode in the potential range (*a*) −0.5 to −1.4 V and (*b*) −0.5 to −1.0 V, Scanning rate 50 mV s^{-1}. The *arrows* indicate scan directions of voltages, (*c*) variation of peak current density I'_c with square root of sweep rate

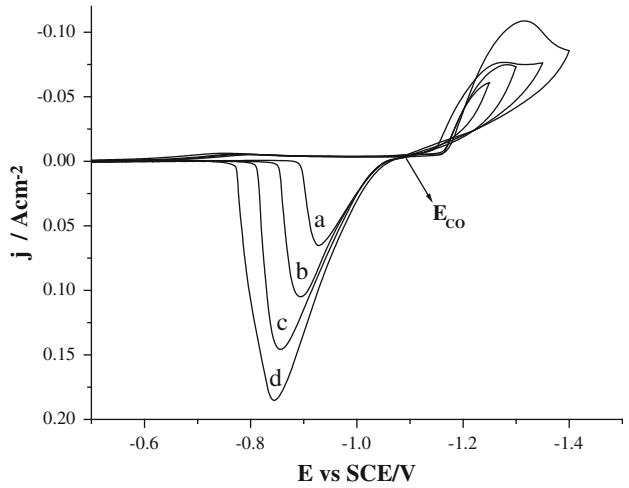

Fig. 4 Typical voltammograms obtained on SS101 stainless steel in solution S_O, showing the crossover potential (*E*co), at different switching potentials (E_λ) (*a*) $E_\lambda = -1.25$, (*b*) $E_\lambda = -1.31$, (*c*) $E_\lambda = -1.35$ V, (*d*) $E_\lambda = -1$ V, and $v = 50$ mV s^{-1}

degree of surface coverage (θ) in the presence of additives was estimated from the equation

$$\theta = \frac{i - i_s}{i} \tag{2}$$

where i and i_s are the current densities without and with additive, respectively. The coverage values are obtained at potentials $E = -1.316$ V (θ_1) and -1.4 V (θ_2) during cathodic scan of the cyclic voltammogram given in Table 5.

The degree of surface coverage θ values obtained at −1.316 V in the presence (Table 5) of CTAB and EV are 0.754 and 0.825, respectively. At −1.4 V the θ values for CTAB and EV are 0.104 and 0.568, respectively, indicating larger surface area of electrode is available for zinc reduction at higher negative potentials. Hence there is a potential-dependent adsorption of additives. In the case of additive mixture θ values are 0.9 at −1.316 V and 0.883 at −1.4 V, respectively. Larger θ values in the presence of mixture indicated higher degree of surface coverage, and the additives showed synergistic effect on adsorption.

A linear relationship between I_p (I'_C) and $v^{1/2}$ was noticed in the presence of additives as shown in Fig. 5c. This linearity indicates that in the presence of additives reduction of zinc is diffusion-controlled that is under mass transfer limit [39, 40].

Further it was noticed from Table 4 that the diffusion coefficient (Randles–Sevcik equation) magnitude decreased in the presence of additives and suggested that the additives decreased the rate of diffusion of zinc ions to the electrode surface. The decrease in value of diffusion coefficient might be due to two reasons. First, the authors Lin and Lu [41] and Wang et al. [42] reported the formation of mononuclear complexes of Zn^{2+} through lone pair of electrons on oxygen atom present in OH and OCH_3 groups of vanillin. Ethyl vanillin has similar structure with C_2H_5 instead CH_3 group, and hence here also it is expected to form the complex with Zn^{2+} ion resulting in the reduction of diffusion coefficient values. In the present case the formation of complex is not possible because of small concentration of EV. The effect of CTAB on zinc deposition is studied by Gomes et al. It is concluded that CTAB gave lower value of diffusion coefficient and was explained by viscosity change and possible formation of complex [11]. But the effect of complexation of additive with Zn(+2) or a solution viscosity change on decrease in diffusion coefficient is negligible due to relatively lower concentrations of surfactants compared to zinc

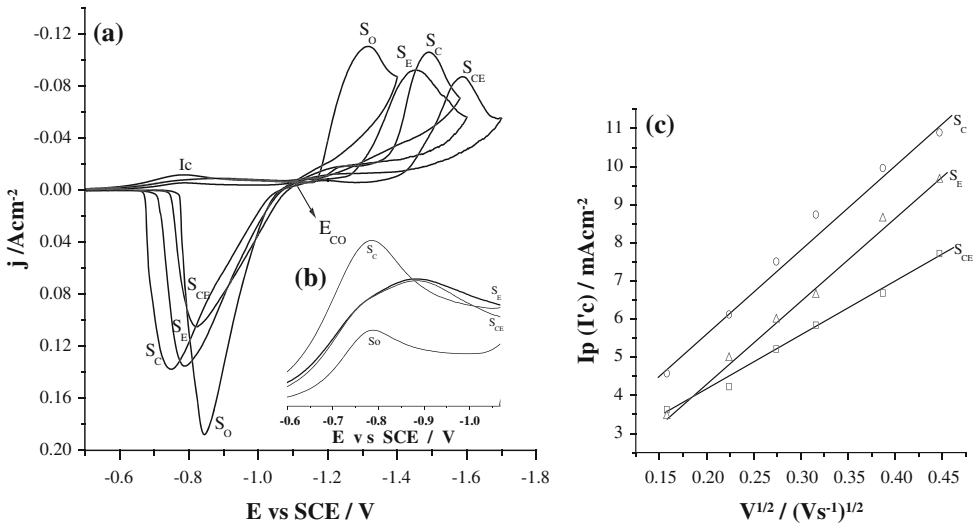

Fig. 5 (*a*) Cyclic voltammograms in the absence and presence of additive, (*b*) hydrogen evolution region in potential range from −0.5 to −1.0 V at $v = 50$ mVs^{-1}, and (*c*) variation of peak current density I'_c with square root of sweep rate

Table 4 Values of the crossover potential (E_{CO}), cathodic peak potential ($E_{I'c}$), and overpotential (η), associated with the reduction of zinc with and without additive on stainless steel electrode

Solutions	E_{CO} vs. S_{CE} (V)	$E_{I'c}$ vs. S_{CE} (V)	$\eta_{I'c}$ (V)	Ip (I'_C)
S_o	−1.095	−1.315	0.220	0.110
S_C	−1.184	−1.495	0.311	0.104
S_E	−1.118	−1.454	0.336	0.099
S_{CE}	−1.121	−1.589	0.468	0.086

Table 5 Values of degree of surface coverage θ and diffusion coefficient D_o

Solutions	θ_1*	θ_2	D_o (10^{-6} cm^2 s^{-1})
S_O			2.230
S_C	0.754	0.104	1.103
S_E	0.825	0.568	0.993
S_{CE}	0.9	0.883	0.353

concentration in the solution. Second, the additive CTAB is adsorbed on the electrode surface. This adsorption is potential-dependent, and it desorbs from electrode surface at more negative potential rendering large surface area available for zinc reduction. Due to adsorption of CTAB on electrode surface the electro-active area available for zinc reduction decreases. If the surface area remaining after adsorption is about 0.0479 cm^2 (two-third) then the diffusion coefficient of Zn^{2+} in the presence of CTAB is 2.48 × 10^{-6} cm^2 s^{-1}. This value is approximately same as that obtained in the absence of additives. At −1.5 V the diffusion coefficient value is found to be 2 × 10^{-6} cm^2 s^{-1} which is much higher than diffusion coefficients obtained at potentials less than −1.5 V [39]. Hence decrease in diffusion coefficient in the presence of CTAB is due to adsorption. Similarly in the presence of EV and CTAB + EV, decrease in diffusion coefficient values is also due to adsorption. The decrease in diffusion coefficient is appreciable in the presence of mixture CTAB + EV and is about 0.353 × 10^{-6} cm^2 s^{-1}. This inferred higher surface coverage through adsorption of additives.

To know the influence of additives on E_{CO}, the voltammograms are recorded for S_O, S_C, S_E, and S_{CE} at different E_λ. E_{CO} values remain constant at different E_λ and are given in Table 4. It is more negative in the presence of additives than in their absence. Decrease in E_{CO} is due to lower concentration of Zn^{2+} ion at the interface. Adsorption of additives on plating surface increases the activation energy required for the Zn^{2+} reduction [37]. E_{CO} shift is more pronounced in the presence of both the additives due to their combined effect.

Table 4 also shows the overpotential values $\eta = E_{I'C} - E_{CO}$, obtained for solutions with and without additives. A higher overpotential value is noticed for S_C, S_E, and S_{CE}, and it is maximum for S_{CE}. The lower peak current is observed for S_{CE} than S_O, S_C, and S_E [43]. This suggests that all additives are effective at the interface. But higher interaction at the interface is observed for the additives mixture. These results indicate that the additive mixture acts at the interface, creating barrier at the vicinity of the electrode and blocking the discharge of metal ions. Owing to this reason higher activation energy is required for deposition of zinc thus exhibiting higher overpotential. The bright deposition is always associated with refinement in its crystal size. The grain refinement is a necessary condition for bright deposition. Here the additives enhanced the deposition overpotential thus responsible for the formation of bright and smooth zinc deposit.

Cetyltrimethylammonium bromide, a cationic surfactant, influences diffusion of zinc ions in aqueous medium, and it gets adsorbed on the electrode surface during plating

thereby causing higher overpotential for deposition. Thus, CTAB generated leveled and fine-grained deposit. EV is hydrophobic in nature, and its solubility in aqueous solution is lower. During plating it gets accumulated on the electrode surface leading to nonuniform deposit. However, the hydrophobic EV easily interacts with CTAB and thus increased the solubility of EV in aqueous medium. These precombined larger molecules effectively get adsorbed and smoothen the deposit surface [30].

3.3 Combined effect of CTAB and EV on the nucleation mechanisms

The primary factor leading to the generation of fine-grain deposit is the formation of fresh nucleation sites and their rate of growth. This information is obtained from the chronoamperometric study. In this study, the potentiostatic transients are recorded in the potential range from −1.1 to −1.6 versus S_{CE}. All the transients properties obtained are typical of a nucleation process, and similar-shaped curves are observed for all solutions. All the curves showed initial sharp rise in short time, and the current reaches a maximum value (i_{max}). This sharp rise in current is probably due to the growth and stabilization of initial nuclei. The decay in current density after reaching i_{max} of each transients converges almost to a limiting current, and nucleation process is controlled by diffusion of zinc ion [20].

The nucleation mechanism is identified by drawing dimensionless curves and compared with those obtained using the model of Schariker and Hills [44] for 3D instantaneous and progressive nucleation processes which are under diffusion control.

The model uses the following equations for identifying 3D instantaneous and progressive nucleation process.

$$\text{Instantaneous Nucleation } \left(\frac{i}{i_m}\right)^2 = 1.9542\left\{1-\exp\left[-1.2564\left(t/t_m\right)\right]\right\}^2\left(t/t_m\right)^{-1} \quad (3)$$

$$\text{Progressive Nucleation } \left(\frac{i}{i_m}\right)^2 = 1.254\left\{1-\exp\left[-2.3367\left(t/t_m\right)^2\right]\right\}^2\left(t/t_m\right)^{-1} \quad (4)$$

where i represents the current density at any instant of time t and i_m is the maximum current density with corresponding time t_m.

Two limiting cases arise here, in the first case, based on Eq. 3, all nuclei are formed immediately after potential step, referred as instantaneous nucleation. In the second case, Eq. 4, the number of nuclei increases during the entire deposition process, referred as progressive nucleation.

The current transients obtained for solution S_O between the potential −1.29 and −1.315 V and the corresponding dimensionless graph are plotted. The experimental results are in agreement with 3D instantaneous nucleation process shown in Fig. 6. Further the transients are recorded at different potentials selected between crossover and peak potentials of solutions S_C, S_E, and S_{CE} which contain CTAB, EV, and their mixture, respectively. The Fig. 7i and ii shows the resulting dimensionless graphs. In the presence of EV, the nucleation process is 3D instantaneous where as in the presence of CTAB, it is 3D progressive. However, in the case of mixture of additives (S_{CE}), the nucleation process is neither instantaneous nor progressive but lies between these two limiting cases.

The Scharifker and Hill model is largely used to discuss the progressive or instantaneous mode of the nucleation reaction, but in practices it is very difficult to extract useful information on kinetic parameters from this model. According to the model given by Scharifker and Mostany [45], it is not necessary to classify the nucleation process in order to obtain kinetic parameter. The following Eq. 5 of Scharifker and Mostany can be employed to calculate the nucleation rate constant per site 'A' and the number density of active site 'N_O' over the electrode surface using experimental current transients.

$$i(t) = \left(\frac{zFD^{1/2}c}{\pi^{1/2}t^{1/2}}\right)\left\{1-\exp\left[-N_O\pi k^* D\left(t-\frac{(1-e^{At})}{A}\right)\right]\right\} \quad (5)$$

where $k^* = (8\pi M/\rho)^{1/2}$, zF is the molar charge of the electrodepositing species, D is the diffusion coefficient in cm s^{-2} (calculated from the falling part of the current transients), c is the bulk concentration, M is the atomic weight of zinc, and ρ is the density of the deposited material. The Tables 6 and 7 list the value of kinetic parameters obtained for solutions S_O, S_C, S_E, and S_{CE} by the nonlinear fitting of Eq. 5. The nucleation rate (A) and number density of active sites (N_O) increase as the potential was changed to more negative; this behavior is characteristic of a diffusion-controlled 3D nucleation process.

The value of N_O and A indicated the influence of additive, either individual or in combination, on nucleation process. The appreciable effect of additives on nucleation parameter is noticed in the presence of mixture rather than their individual presence.

Further, the nucleation rate A that is larger for S_O indicates low number of active sites on the surface which becomes exhausted at early stages of the process and followed instantaneous nucleation. The same trend is observed in the presence of EV. However, the presence of CTAB (S_C) shows the nucleation parameters, smaller A, and larger N_O, which closely followed the response

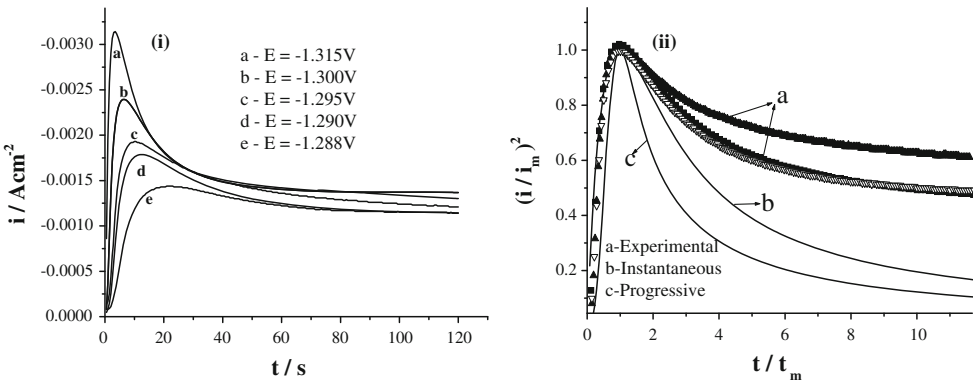

Fig. 6 **i** Typical family of potentiostatic current density transients for the nucleation of Zn for solution So on stainless steel at different overpotentials, **ii** nondimensional plots for 3D nucleation

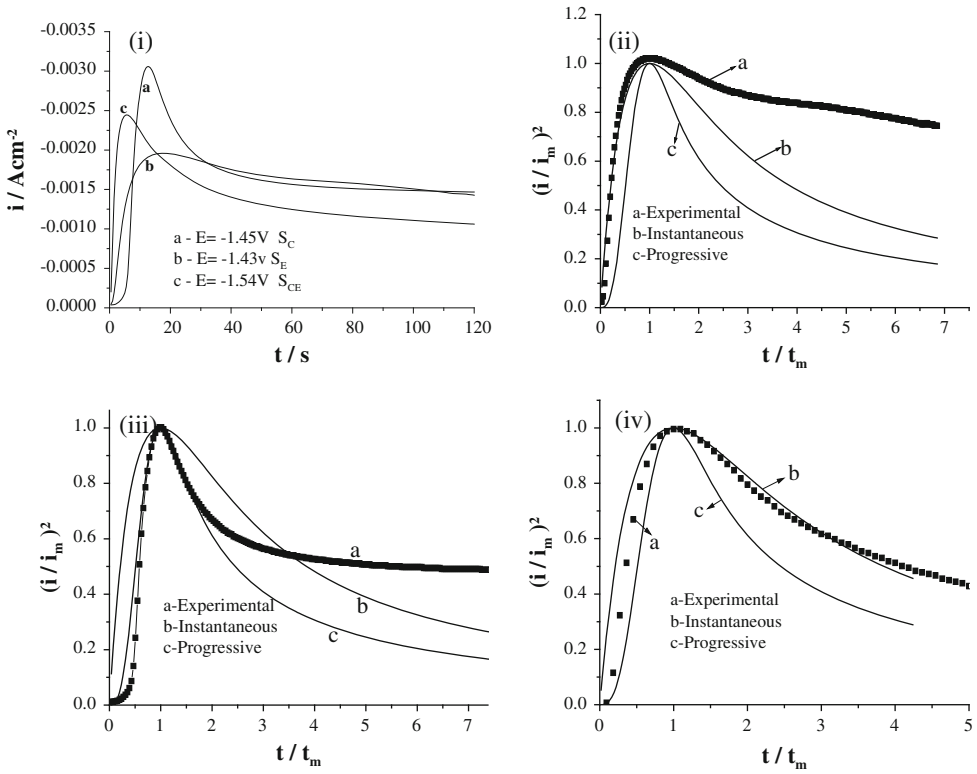

Fig. 7 **i** Typical family of potentiostatic current density transients for the nucleation of Zn for solution S_C, S_E and S_{CE} on stainless steel at different overpotentials and nondimensional plots for (3D nucleation) solutions, **ii** S_E, **iii** S_C, and **iv** S_{CE}

Table 6 Kinetic parameters extracted from the nonlinear fitting of Eq. 5 to current transients obtained for solutions S_O and S_C

Solution S_O					Solution S_C				
$-E$ vs. S_{CE} (V)	t_m (s)	i_m (mA cm^{-2})	N_O (10^5 cm^{-2})	A (s^{-1})	$-E$ vs. S_{CE} (V)	t_m (s)	i_m (mA cm^{-2})	N_O (10^5 cm^{-2})	A (s^{-1})
−1.27	21.79	1.44	0.78	0.078	−1.4	19.42	2.43	2.76	0.027
−1.28	12.29	1.79	0.85	0.26	−1.43	16.04	2.85	3.35	0.033
−1.29	10.33	1.92	0.95	0.37	−1.45	12.66	3.06	5.61	0.031
−1.300	6.45	2.39	1.39	0.68	−1.46	8.22	3.32	6.49	0.064
−1.315	3.80	3.14	1.76	6.89					

predicted for progressive nucleation wherein the number of active sites increased. But in the mixture (EV + CTAB), still higher value of N_O and smaller value of A are noticed. This indicated blocking effect of additives, which contributes to the existence of larger fraction of sites, becomes active with increased cathodic overpotential [46].

Table 7 Kinetic parameters extracted from the nonlinear fitting of Eq. 5 to current transients obtained for solutions S_E and S_{CE}

Solution S_E					Solution S_{CE}				
$-E$ vs. S_{CE} (V)	t_m (s)	i_m (mA cm$^{-2)}$	N_O (10^5 cm^{-2})	A (s^{-1})	$-E$ vs. S_{CE} (V)	t_m (s)	i_m (mA cm^{-2})	N_O (10^5 cm^{-2})	A (s^{-1})
−1.42	19.36	1.71	0.92	0.129	−1.45	28.86	1.30	3.54	0.026
−1.43	17.61	1.96	1.01	0.143	−1.49	11.67	1.57	6.14	0.0
−1.44	15.21	2.23	1.17	0.165	−1.53	9.25	1.97	7.75	0.057
−1.45	12.31	2.64	1.45	0.204	−1.54	6.90	2.19	10.39	0.077
					−1.55	5.65	2.44	12.68	0.094

4 Conclusion

The nanosized bright crystalline zinc deposit was obtained from sulfate electrolyte containing both ethyl vanillin and cetyltrimethylammonium bromide. The deposit transformed from dull appearance (without additives) to smooth fully bright appearance in the presence of both additives. The zinc-preferred orientation also changed to (100) (110) in the presence of additives. The additives when present together produce good zinc deposit with high surface reflectance of 85%.

The peak potential corresponding to zinc reduction is always negative in the presence of additives than their absence. Higher shift is observed for additive mixture and accounts for fine-grained nature of bright deposit. The additives adsorb on the steel surface (shift of E_{CO} toward negative direction) and create diffusion condition. The chronoamperometric study supports the combined effect of CTAB and EV on nucleation mechanism. The additives increased the number of active sites and decreased the rate of nucleation, which results in refinement of grain size.

Acknowledgments The authors are grateful to University Grant Commission, New Delhi, Govt. of India for providing financial assistance (Project No. F. No. 32-220/2006(SR) Dated: 24/03/2007), and Department of Chemistry, Kuvempu University for providing laboratory facilities.

References

1. Arthoba Naik Y, Venkatesha TV (2005) Bull Mater Sci 28:495
2. Arthoba Naik Y, Venkatesha TV, Nayak PV (2002) Turk J Chem 26:725
3. Shanmugasigamani S, Pushpavanam M (2006) J Appl Electrochem 36:315
4. Muralidhara HB, Arthoba Naik Y (2006) Surf Coat Technol 202:3438
5. Kavith B, Santhosh P, Renukadevi M, Kalpana A, Shakkthivel P, Vasudevan T (2006) Surf Coat Technol 201:3438
6. Schneider HS (1977) Plat Surf Finish 64:52
7. Loshkarev YuM, Livshits AB, Snetkova LP, Gorlova MS, Stupakevich BV (1972) Issled Elektroosayhdeniyu Rastvoreniyu Metal (Frumkin AN ed), 132, "Nauka", Moscow (1972); Chem Abstr 76:29975b
8. Loshkarev MA, Boichenko LM, Nesterenko AF (1971) & (1972) Khim Tekhnol (Kharkov) 18:33; Chem Abstr 76:8002j
9. Li M, Luo S, Qian Y, Zhang W, Jiang L, Shen J (2007) J Electrochem Soc 154(11):D567
10. Lee J-Y, Kim J-W, Lee M-K, Shin H-J, Kim H-T, Parka S-M (2004) J Electrochem Soc 151(1):C25
11. Kim J-W, Lee J-Y, Park S-M (2004) Langmuir 20:9
12. Mockute D, Bernotiene G- (1997) J Appl Electrochem 27:691
13. Li MC, Jiang LL, Zhang WQ, Qian YH, Luo SZ, Shen JN (2007) J Solid State Electrochem 11:549
14. Kim S-J, Kim H-T, Parka S-M (2004) J Electrochem Soc 151(12):C850
15. Kardos O Plating 61(1974),(2)129;(3)229: (4) 316
16. Boto K (1975) Electrodeposition Surf Treat 3:77
17. Diaz-Arista P, Meas Y, Ortega R, Trejo G (2005) J Appl Electrochem 35:217
18. Gomes A, da Silva Pereira MI (2006) Electrochim Acta 52:863
19. Gomes A, da Silva Pereira MI (2006) Electrochim Acta 51:1342
20. Ballesteros JC, Dıaz-Arista P, Meas Y, Ortega R, Trejo G (2007) Electrochim Acta 52:3686
21. Oniciu L, Muresan L (1991) J Appl Electrochem 2:565
22. Ravindran V, Muralidharan VS (2000) Bull Electrochem 16:60
23. Youssef KhMS, Koch CC, Fedkiw PS (2004) J Electrochem Soc 151:C103
24. Mockute D, Bernotiene G (2000) Surf Coat Technol 135:42
25. Saber Kh, Koch CC, Fedkiw PS (2003) Mater Sci Eng A 341:174
26. Paunovic M, Schlesinger M (1998) Fundamentals of electrochemical deposition electrochemical society series. Wiley, New York, p 53
27. Cullity BD (1978) Elements of X-ray diffraction, 2nd edn. Addision-Wesley Publishing Company, Inc., Philippines
28. Mouanga M, Ricq L, Douglade J, Bercot P (2007) J Appl Electrochem 37:283
29. Lide DR (2005) CRC handbook of chemistry and physics, 81st edn. CRC Press, Boca Raton, LLC, pp 5–93
30. Hsieh J-C, Hu C-C, Lee T-C (2008) J Electrochem Soc 155:D675
31. Reddy AKN (1963) J Electroanal Chem 6:141
32. Casanova T, Soto F, Eyraud M, Crousier J (1997) Corr Sci 39:529
33. Cachet C, Wiart R (1994) J Electrochem Soc 141:131
34. de Oliveira EM, Carlos IA (2008) J Appl Electrochem 38:1203
35. Zhang Z (2001) Trans Nonferr Met Soc China 11(4):603
36. Trejo G, Ortega R, Meas Y, Ozil VP, Chainet E, Nguyen B (1998) J Electrochem Soc 1:4090
37. Fletcher S, Halliday CS, Gates D, Westcott M, Lwin T, Nelson G (1983) J Electroanal Chem 159:267
38. Kladekova D, Lova MG, Pikna LR (2005) Particulate Sci Technol 23:189

39. Barry FJ, Cunnane VJ (2002) J Electroanal Chem 537:151
40. Trejo G, Ruiz H, Ortega Bores R, Meas Y (2001) J Appl Electrochem 31:685
41. Lin ZD, Lu JY (2005) Acta Cryst E61:743
42. Wang AD, Bi CF, Fan YH, Zou YN, Xu JK, Kan YH (2008) Russ J Coord Chem 34(8):475
43. Pereira MS, Barbosa LL, Souza CAC, De Moraes ACM, Carlos IA (2006) J Appl Electrochem 36:727
44. Scharifker BR, Hills G (1983) J Electochem Acta 28:879
45. Scharifker BR, Mostany J (1984) J Electroanal Chem 177:13
46. Alvarez AV, Salinas DR (2004) J Electroanal Chem 566:393